ACS Catalysis

Letter

pubs.acs.org/acscatalysis

Kinetic Enhancements in DNA−Enzyme Nanostructures Mimic the Sabatier Principle

Jyun-Liang Lin and Ian Wheeldon*

Department of Chemical and Environmental Engineering, University of California, Riverside, Bourns Hall, 900 University Avenue, Riverside, CA 92521, United States

Supporting Information

ABSTRACT: Advances in DNA bionanotechnology have led to the ability to create structures with well-defined chemical and physical features at the nanoscale. Such nanostructures can be used to create spatially organized enzymatic cascades that promote substrate channeling and result in enhanced cascade kinetics. Here, we investigate the effects of substrate−scaffold interactions on the catalytic activity of an enzyme−DNA complex using horseradish peroxidase (HRP) and a nanoscale DNA scaffold with three addressable sites. Kinetic assays with a library of HRP substrates revealed that DNA scaffolding enhances HRP activity in a manner that is analogous to the Sabatier Principle. In this case, the binding of the substrate is to the scaffold and not to the catalyst, but the Sabatier trend holds: weak and strong binding substrates showed no enhancement in kinetics, whereas intermediately bound substrates result in >300% increase in enzyme activity.

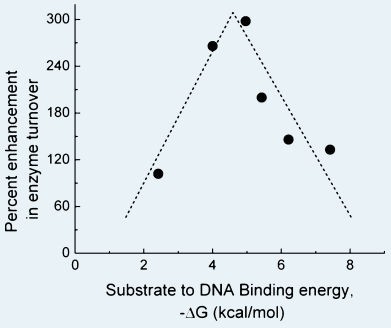

KEYWORDS: *nanostructures, enzymes, DNA interactions, Sabatier, horseradish peroxidase*

Metabolic pathways are often organized in multienzyme complexes that promote the efficient transport and processing of substrates along the pathway, resulting in enhanced pathway kinetics and high yields.[1,2] When engineering new and re-engineering existing pathways, such nanoscale organization and the associated kinetic benefits are often lost. A number of recent efforts to reproduce these kinetic benefits in engineered pathways, both in vitro and in vivo, have focused on enzyme colocalization with nucleic acid[3−7] and protein scaffolding,[8−10] where scaffold is defined as a biomolecular structure to which proteins can be attached at specific sites. As a material, DNA can be used to create precisely defined multidimensional shapes with molecular-level control over structural and chemical features.[11] These capabilities can be used to create multienzyme cascades (or polyvalent enzyme displays) with well-defined spatial organization. However, interactions between enzyme substrates and scaffolds, and their potential effects—beneficial or detrimental—on enzyme kinetics have yet to be explored. Here, we investigate a potentially advantageous (or constraining) aspects of these designs, interactions between substrates and the DNA scaffold.

On the basis of well-known interactions between small molecules and DNA (e.g., DNA stains used in electrophoresis and anticancer drugs[12,13]) and DNA templating of aniline monomers for the enzyme-mediated synthesis of polyaniline nanowires,[14] we reasoned that interactions between DNA scaffolds and enzyme substrates may affect local substrate concentrations and alter the kinetics of enzymes assembled in enzyme-DNA nanostructures. To investigate this possibility, we used a model system of horseradish peroxidase (HRP) assembled on a nanoscale DNA triangle. We elected to use this system because HRP oxidizes a wide range of chemically distinct substrates, including phenol; charged and uncharged phenolics; and colorimetric substrates, such as 2,2′-azino-bis(3-ethylbenzothiazoline-6-sulfonic acid) (ABTS) and 3,3,5,5-tetramethylbenzidine (TMB) that are commonly used in analytical assays. This range of substrates differs in their interactions with DNA, binding with a range of affinity and location thus allowing for experimental investigation of enzyme kinetics with varying substrate−scaffold interactions.

One, two, and three HRPs were assembled on a triangular DNA scaffold (Figure 1a). The scaffold design was based on a previously demonstrated DNA nanostructure[15] and was modified in this work to reduce each side of the structure to ∼25 nm in length. This scaffold was selected because its tensegrity design maintains a rigid structure, the structure has high assembly efficiency, and it has the potential to be used as a scaffold for the controlled assembly of reaction cascades with two and three enzymes. HRP was first conjugated with the thiol-terminated, 10-base, single-stranded DNA oligomer, A1, with the bifunctional cross-linker Sulfo-succinimidyl-4-(*N*-maleimido-methyl)-cyclohexane-1-carboxylate (Sulfo-SMCC). Purified HRP−A1 conjugates were mixed with triangular DNA scaffolds with one, two, or three complementary sticky ends (unhybridized 10-base segments) to produce enzyme−DNA nanostructures with one, two, and three HRPs on the points of the triangular scaffold (HRP_1−, HRP_2−, and HRP_3−DNA, respectively). For detailed preparation of DNA scaffolds

Received: November 28, 2012
Revised: February 12, 2013
Published: February 19, 2013

   dx.doi.org/10.1021/cs300766d | *ACS Catal.* 2013, 3, 560−564

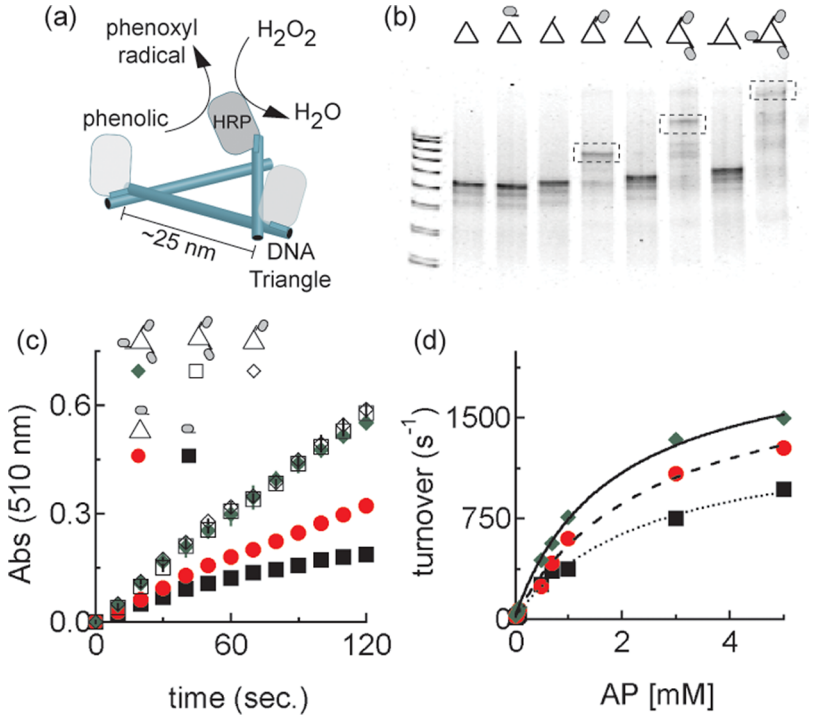

Figure 1. Kinetic enhancement of HRP–DNA nanostructures. (a) Illustration of HRP–DNA nanostructures, indicating that structures with 1, 2, and 3 HRP may be present. (b) Electrophoretic mobility shift assay of HRP_n–DNA nanostructures with 4–15% polyacrylamide native gel: lane 1, DNA ladder (increments of 100 bp from 200 to 1000); 2, DNA triangle (DNA); 3, DNA with unassembled HRP–A1; 4, DNA with 1-sticky end; 5, HRP_1–DNA; 6, 2-sticky end DNA; 7, HRP_2–DNA; 8, 3-sticky end DNA; 9, HRP_3–DNA. (c, d) Product formation as a function of time and turnover number as a function of substrate concentration for $HRP_{1,2,3}$–DNA nanostructures and freely diffusing and unassembled enzyme controls.

and enzyme–DNA assemblies, see Materials and Methods, SFigures 1 and 2, and STable 1 in the Supporting Information. Figure 1b shows the successful assembly of HRP_1–, HRP_2–, and HRP_3–DNA by electrophoretic mobility shift assay. Lanes 5, 7, and 9 (numbered from left to right) show distinct bands of increasing molecular weight that correspond to HRP_1–, HRP_2–, and HRP_3–DNA, respectively. Shifts in DNA bands were not observed in the absence of HRP–A1 or when the scaffold did not display sticky ends (Figure 1b, lane 3). The shift assay reveals that assembly of each structure results in a mixed population of scaffolds with no attached enzymes and scaffolds with one, two, and three HRPs attached when applicable. Assembly yield of HRP_1–DNA, determined by image analysis of the shift assays, was found to be 0.57 (lane 5), whereas HRP_2– and HRP_3–DNA were assembled with yields of 0.34 and 0.30 (lanes 7 and 9), respectively.

To explore whether HRP kinetics are affected by substrate–scaffold interactions, we first used *p*-aminophenol (AP) as a substrate. AP has potential for electrostatic and hydrogen bonding interactions with the negatively charged DNA scaffolds and is readily oxidized by HRP at pH below the pK_a of the primary amine para to the phenolic hydoxy group (pK_a = 5.29).[16] The activity of HRP–DNA nanostructures as well as unbound HRP–A1 in the presence of the scaffold and freely diffusing HRP–A1 controls were determined by measuring the absorbance of the quinoneimine dye product of oxidized AP and 4-aminoantipyrine at 510 nm at pH 5.[17] In kinetic assays of equal enzyme concentrations, HRP_3–DNA showed a clear increase in initial activity over freely diffusing HRP–A1 and unassembled HRP–A1 and DNA scaffold (Figure 1c). The initial rate of AP oxidation with HRP_3–DNA (uncorrected for yield) was found to be 1182 ± 166 s^{-1} (mean ± SD), whereas initial rates of HRP–A1 in the presence and absence of DNA scaffold were 775 ± 18 and 493 ± 42 s^{-1}, respectively. The initial rates of HRP_1– and HRP_2–DNA were found to be equal to that of HRP_3–DNA (Figure 1c).

Since similar specific activities were observed in all HRP–DNA nanostructures, HRP_3–DNA was selected for all subsequent studies, including the determination of the apparent Michaelis–Menten constant (K_M) and turnover number (k_{cat}). The apparent K_M of HRP_3–DNA was 1.8 ± 0.1 mM, smaller than both the unbound and freely diffusing HRP–A1 with K_M of 2.6 ± 0.4 and 2.5 ± 0.3 mM, respectively, suggesting that DNA scaffolds increased the affinity of AP to HRP. In addition, the k_{cat} of HRP_3–DNA was significantly greater than the freely diffusing control (HRP_3–DNA, k_{cat} = 2100 ± 60 s^{-1}; freely diffusing HRP–A1, k_{cat} = 1420 ± 90 s^{-1}). Although initial rates of the HRP_3–DNA are greater than the unassembled control, fits to the rate data yield k_{cat} values that are statistically similar. Increased turnover of HRP with phenolic substrates at concentrations above and below their respective K_M values have also been observed in the presence of excess calf thymus DNA in solution.[18] Changes in K_M and k_{cat} for DNA modified heme centers in HRP has also been reported.[19] The increase in turnover in the presence of DNA was also observed in our system (i.e., the unassembled control), possibly as a result of interactions between the positively charged HRP (*p*I = 8.8) and negatively charged DNA .

If the observed enhancement in specific activity was due solely to electrostatic interactions between the negatively charged phosphate backbone of DNA and the positively charged amino group of AP, the enhancement should be suppressed in the presence of salt. Here, we define the percent enhancement of enzyme activity as the ratio of the specific

dx.doi.org/10.1021/cs300766d | *ACS Catal.* 2013, 3, 560–564

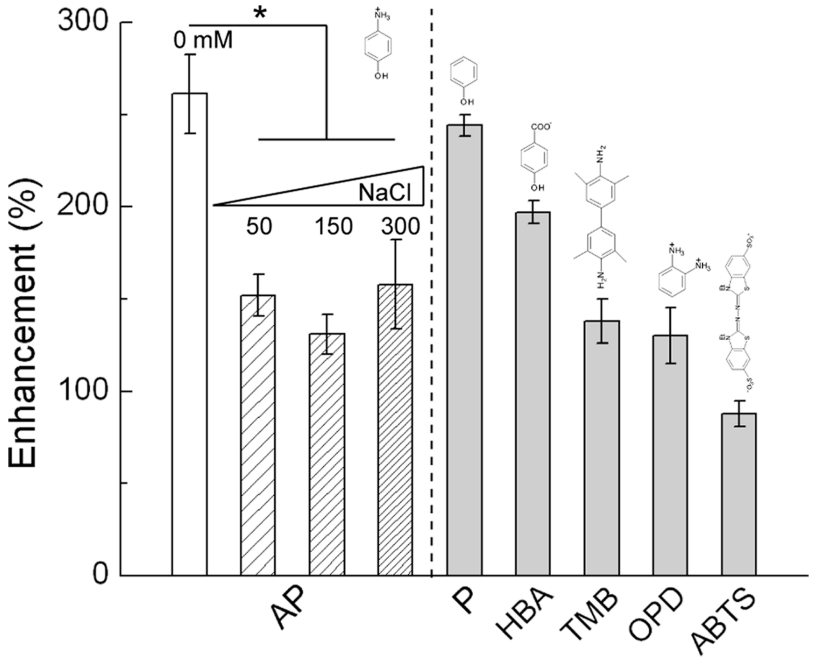

Figure 2. Kinetic enhancement of DNA scaffolded HRP is salt concentration- (left) and substrate-dependent (right). Percent enhancement is defined as the ratio of the initial rate of the HRP_3–DNA nanostructure over the initial rate of freely diffusing HRP modified with a 10-base oligomer. Error bars are standard deviation ($n \geq 3$, * $p \leq 0.05$).

activity of the HRP_n–DNA nanostructure over the specific activity of HRP–A1[4] with substrate and H_2O_2 concentrations 2–3 times the expected K_M values (ref 17 and Supporting Information STable 2). Figure 2 (left) shows the kinetic enhancement decreased to 153 ± 21, 131 ± 11, and 158 ± 24% in the presence of 50, 150, and 300 mM NaCl, respectively (Supporting Information SFigure 3), suggesting that electrostatics is in part responsible for the effect and that other interactions may also be present. In support of nonelectrostatic interactions, an increase in activity of 244 ± 6% was observed with phenol (P; Figure 2, right, Supporting Information SFigure 4). In addition, the phenolic substrate *p*-hydroxybenzoic acid (HBA), which has a negatively charged carboxylic acid group in place of the positively charged amino group on AP, showed a 197 ± 6% enhancement in activity. With two positively charged amino groups, the enhancement in activity (130 ± 16%) with the nonphenolic substrate, *o*-phenylenediamine (OPD), was much smaller than that of AP, also suggesting a partial role of electrostatics in the enhancement. The kinetic enhancement of TMB, which is also positively charged, was found to be 138 ± 12%. Finally, the common HRP substrate ABTS resulted in a slightly reduced activity (88 ± 7%), possibly due to its negative charge. A control sample with a 50 bp double-stranded DNA oligomer conjugated to HRP also yielded enhanced activity (174 ± 12%; Supporting Information SFigure 5), indicating that the scaffold structure was relevant to the enhanced activity.

Substrate binding to the DNA scaffold was analyzed by molecular docking simulations of each substrate to the 10-bp double-stranded DNA fragment closest to the immobilized enzyme (i.e., DNA oligomer A1). Simulations with AutoDock software predicted stable docking poses and a corresponding binding energy (consisting of van der Waals, hydrogen bonding, desolvation, electrostatic, and torsional energies).[20] With the exception of OPD, all substrates were predicted to bind preferentially in the minor groove of the DNA double helix (Figure 3a and Supporting Information SFigure 6). OPD bound to the phosphate backbone bridging the major and minor grooves and bound with higher affinity than all other substrates (OPD, $\Delta G = -7.42$ kcal/mol, $k_d = 4$ μM). TMB also bound strongly to the double-stranded DNA segment ($\Delta G = -6.21$ kcal/mol, $k_d = 28$ μM), whereas ABTS bound weakly in the minor groove ($\Delta G = -2.72$ kcal/mol, $k_d = 10$ mM). The phenolic substrates also bound in the minor groove with the rank order from strongest to weakest of HBA, AP, and P (HBA, AP, and P, $\Delta G = -5.43$, -4.96, and -4.00 kcal/mol and k_d = 104, 231, and 1160 μM, respectively). Interestingly, the substrates with the highest and lowest affinity showed little, if any, enhancement in activity.

A well-known concept in heterogeneous catalysis is the Sabatier Principle, which states that binding between substrate and catalyst should be "just right", that is, substrate binding to the catalyst should not be too weak or too strong.[21] Weakly binding substrates fail to associate with the catalyst, resulting in no reaction, and strongly bound substrates are slow to dissociate and prevent reaction by blocking active sites. This concept is graphically shown by plotting reaction rate as a function of heat of formation of the adsorbate. The result is a volcano plot, so-called as the maximum of a parabolic (or triangular) fit to the data peaks at the optimum binding energy and maximum reaction rate.[22]

This trend is mimicked here with the enhancement of enzyme activity resembling a volcano plot. Figure 3b shows the kinetic enhancement for each substrate (corrected for HRP_3–DNA assembly yield; see Materials and Methods in the Supporting Information) as a function of the substrate–DNA binding energy. Substrates that bind weakly and strongly to the scaffold showed little to no enhancement. The maximum enhancement resulted from an intermediate binding energy between scaffold and substrate. It is important to emphasize that the Sabatier Principle is only mimicked and not reproduced. The effect is one of kinetic enhancement in

dx.doi.org/10.1021/cs300766d | ACS Catal. 2013, 3, 560–564

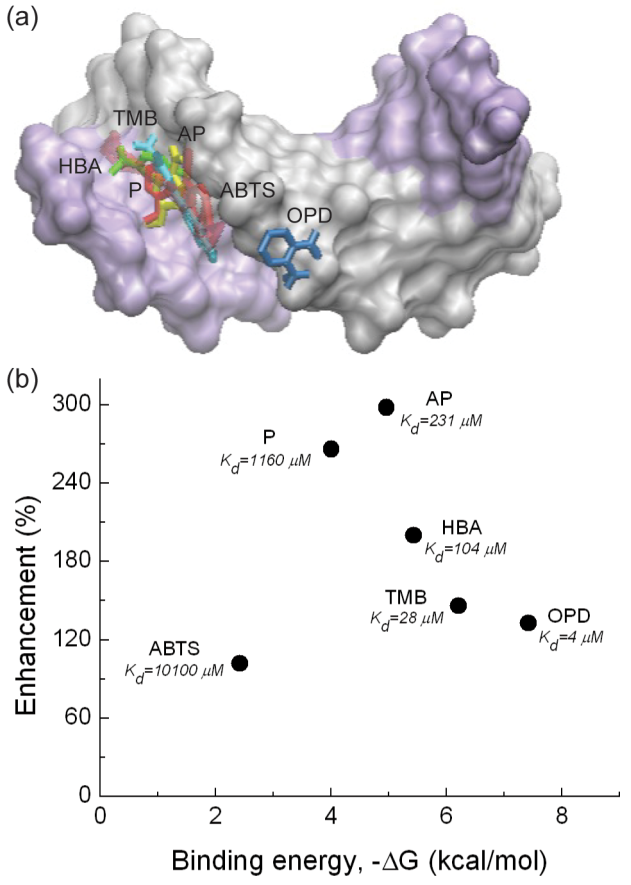

Figure 3. Kinetic enhancements in HRP–DNA nanostructures mimic the Sabatier principle. (a) Molecular model of putative binding sites for each substrate on DNA: P, red; AP, yellow; HBA, green; OPD, blue; TMB, cyan; and, ABTS, faint red. Molecular docking to the 10-base-pair sequence closest to the immobilized enzymes was performed by AutoDock. One strand of the double-stranded DNA is colored gray, the other strand is colored purple. (b) The enhancement of HRP activity (corrected for HRP_3–DNA assembly yield) as a function of the predicted substrate–DNA binding energy. Calculated binding constants for each substrate are shown as data labels.

enzyme–DNA nanostructures and not absolute reaction rate, as is traditionally shown in volcano plots. In addition, the observed effect is analogous to the true Sabatier Principle. We ascribe the observed effect to an increase in concentration of the substrate localized around the DNA scaffold in close proximity to the attached enzyme, an effect that is supported by the decrease in apparent K_M of AP (Figure 1d).

Regardless of the mechanisms that bring about the trend in kinetic enhancement (Figure 3), the kinetic data of multiple substrates oxidized by HRP assembled on a DNA scaffold clearly shows that scaffold–substrate interactions can affect the overall performance and functioning of the system. In the case presented here, the interactions between enzyme substrate and scaffold are mostly beneficial: enzyme turnover was increased, and the apparent Michaelis binding constant (K_M) was reduced. This observation has potential implications in designing multienzyme reaction cascades with nucleic acid scaffolds,[3−7,11] and will also affect the design of addressable DNA scaffolds for protein nanoarrays,[23,24] DNA origami-based drug delivery systems,[25] and the design and application of DNA-based materials in general. More specifically, our observations that the apparent turnover and binding constant may be altered when enzymes (or binding proteins) are assembled on nonchemically inert scaffolds suggest that (i) the kinetics and ligand binding should be characterized after assembly of the system, (ii) the changes may be substrate- and scaffold-dependent, and (iii) it may be possible to exploit the binding properties of the scaffold to increase local concentration of substrates and, in the case of couple reactions, increase the local concentration of reaction intermediates.

In this work, we have designed and created a nanoscale triangular DNA scaffold to polyvalently display up to three HRP enzymes. We used this system to investigate potential effects on enzyme kinetics due to substrate–scaffold interactions. Phenolic compounds (P, AP, and HBA) were oxidized at enhanced rates over unassembled HRP modified with a 10-bp, single-stranded DNA oligomer. Other substrates, including ABTS and OPD, and TMB showed little to no enhancement in rate with DNA-scaffolded HRP. Plots of the kinetic enhancement as a function of the predicted binding energy of the substrate to the 10-bp closest to the immobilized enzyme revealed a trend that mimics the Sabatier Principle in heterogeneous catalysis. These observations have implications on the design and application of multienzyme nanostructures assembled with DNA scaffolds and with DNA bionano materials in general.

■ ASSOCIATED CONTENT

Supporting Information

Materials and Methods, purification of enzyme–DNA conjugates, DNA scaffold sequences and assembly, HRP kinetic parameters, kinetic assays of salt-dependent experiments, assays of enzyme–DNA constructs with all substrates, double-stranded DNA control assembly and kinetic assay, predicted docking poses of substrates on a double stranded DNA fragment, Figures S1–S6, and Tables S1–S2. This material is available free of charge via the Internet at http://pubs.acs.org.

■ AUTHOR INFORMATION

Corresponding Author

*E-mail: iwheeldon@engr.ucr.edu.

Notes

The authors declare no competing financial interest.

■ ACKNOWLEDGMENTS

This study was supported by the Bourns College of Engineering at the University of California, Riverside. We thank Phil Christopher for his comments and discussion.

■ REFERENCES

(1) Miles, E. W.; Rhee, S.; Davies, D. R. *J. Biol. Chem.* **1999**, *274*, 12193–12196.
(2) Conrado, R. J.; Varner, J. D.; DeLisa, M. P. *Curr. Opin. Biotechnol.* **2008**, *19*, 492–499.
(3) Wilner, O. I.; Weizmann, Y.; Gill, R.; Lioubashevski, O.; Freeman, R.; Willner, I. *Nat. Nanotechnol.* **2009**, *4*, 249–254.
(4) Fu, J. L.; Liu, M. H.; Liu, Y.; Woodbury, N. W.; Yan, H. *J. Am. Chem. Soc.* **2012**, *134*, 5516–5519.
(5) Muller, J.; Niemeyer, C. M. *Biochem. Biophys. Res. Commun.* **2008**, *377*, 62–67.
(6) Delebecque, C. J.; Lindner, A. B.; Silver, P. A.; Aldaye, F. A. *Science* **2011**, *333*, 470–474.
(7) Conrado, R. J.; Wu, G. C.; Boock, J. T.; Xu, H.; Chen, S. Y.; Lebar, T.; Turnsek, J.; Tomsic, N.; Avbelj, M.; Gaber, R.; Koprivnjak, T.; Mori, J.; Glavnik, V.; Vovk, I.; Bencina, M.; Hodnik, V.; Anderluh,

G.; Dueber, J. E.; Jerala, R.; Delisa, M. P. *Nucleic Acids Res.* **2011**, *40*, 1879−1889.
(8) Dueber, J. E.; Wu, G. C.; Malmirchegini, G. R.; Moon, T. S.; Petzold, C. J.; Ullal, A. V.; Prather, K. L. J.; Keasling, J. D. *Nat. Biotechnol.* **2009**, *27*, 753−U107.
(9) You, C.; Myung, S.; Zhang, Y. H. P. *Angew. Chem.* **2012**, *124*, 8917−8920.
(10) Agapakis, C. M.; Ducat, D. C.; Boyle, P. M.; Wintermute, E. H.; Way, J. C.; Silver, P. A. *J. Biol. Eng.* **2010**, *4*, 3.
(11) Fu, J.; Liu, M.; Liu, Y.; Yan, H. *Acc. Chem. Res.* **2012**, *45*, 1215−1226.
(12) Neidle, S. *Nat. Prod. Rep.* **2001**, *18*, 291−309.
(13) Palchaudhuri, R.; Hergenrother, P. J. *Curr. Opin. Biotechnol.* **2007**, *18*, 497−503.
(14) Ma, Y.; Zhang, J.; Zhang, G.; He, H. *J. Am. Chem. Soc.* **2004**, *126*, 7097−7101.
(15) Liu, D.; Wang, M.; Deng, Z.; Walulu, R.; Mao, C. *J. Am. Chem. Soc.* **2004**, *126*, 2324−2325.
(16) Marin, A.; Barbas, C. *J. Pharm. Biomed. Anal.* **2006**, *40*, 262−270.
(17) Feng, J. Y.; Liu, J. Z.; Ji, L. N. *Biochimie* **2008**, *90*, 1337−1346.
(18) Datta, S. G.; Dou, X. Z.; Shibley, A.; Datta, B. *Int. J. Biol. Macromol.* **2012**, *50*, 552−557.
(19) Glettenberg, M.; Niemeyer, C. M. *Bioconjugate Chem.* **2009**, *20*, 969−975.
(20) Morris, G. M.; Goodsell, D. S.; Halliday, R. S.; Huey, R.; Hart, W. E.; Belew, R. K.; Olson, A. J. *J. Comput. Chem.* **1998**, *19*, 1639−1662.
(21) Knözinger, H.; Kochloefl, K. In *Ullmann's Encyclopedia of Industrial Chemistry*; Wiley-VCH Verlag GmbH & Co. KGaA: Weinheim, 2005.
(22) Balandin, A. A. *Adv. Catal.* **1969**, *19*, 1−210.
(23) Sacca, B.; Meyer, R.; Erkelenz, M.; Kiko, K.; Arndt, A.; Schroeder, H.; Rabe, K. S.; Niemeyer, C. M. *Angew. Chem., Int. Ed.* **2010**, *49*, 9378−9383.
(24) Chhabra, R.; Sharma, J.; Ke, Y.; Liu, Y.; Rinker, S.; Lindsay, S.; Yan, H. *J. Am. Chem. Soc.* **2007**, *129*, 10304−10305.
(25) Zhao, Y.-X.; Shaw, A.; Zeng, X.; Benson, E.; Nyström, A. M.; Högberg, B. *ACS Nano* **2012**, *6* (10), 8684−8691.